NON-LINEAR FORCE-FREE MAGNETIC FIELDS.

Thomas Wiegelmann

Max-Planck-Institut für Sonnensystemforschung, 37191 Katlenburg-Lindau, Germany

ABSTRACT

The solar magnetic field is an important quantity which couples the solar interior with the photosphere and atmosphere. Knowledge regarding the coronal magnetic field plays a key role for eruptive phenomena, e.g. coronal mass ejection, flares and eruptive prominences. We describe a computer code for a non-linear force-free extrapolation of photospheric measurements into the corona based on an optimization principle.

We test the accuracy and performance of the method with help of a semi-analytic non-linear force-free equilibrium. Here, we apply the code to data from IVM in Hawaii and SFT in Tokyo.

Key words: magnetic fields, corona, extrapolations.

1. INTRODUCTION

A good knowledge of the coronal magnetic field is necessary to understand and predict basic processes like coronal mass ejections and flares. A magnetic field reconstruction in the solar corona has to be consistent with the observed spatial variation of the coronal plasma (density, pressure, temperature) often elongated along the magnetic field. Unfortunately the coronal magnetic field cannot be measured directly with sufficient accuracy. It is therefore necessary to extrapolate the coronal magnetic field from photospheric measurements.

The magnetic field reconstruction in the solar corona depends on assumptions about the coronal current distribution. Popular simplifications are potential (current free) fields (e.g. Schmidt (1964); Semel (1967)) and linear force free fields (e.g. Chiu and Hilton (1977); Seehafer (1978)). Potential fields and linear force-free fields do not contain free energy and are very probably a poor approximation for active region fields prior to an eruption. The calculation of non-linear force-free fields (e.g. Sakurai (1981); Wheatland et al. (2000); Yan and Sakurai (2000); Wiegelmann and Neukirch (2003); Wiegelmann (2004); Valori et al. (2005)) is complicated by the intrinsic non-linearity of the underlying mathematical problem. From the observational point of view the non linear reconstruction is also more challenging because photospheric vector magnetograph data are required. In future, SOLIS and the Solar-B spacecraft will be ideal instruments for this purpose.

The connectivity of the coronal magnetic field can be seen in 2D projection by e.g. TRACE or EIT. EUV-observations of coronal loop structures will be supplied by STEREO from two viewpoints in space. A 3D stereoscopic reconstruction of these structures is possible in only a limited number of cases. A combined loop and field reconstruction promises to be much more powerful.

2. OPTIMIZATION CODE WITH WEIGHTING FUNCTIONS

2.1. Basic equations

Force-free coronal magnetic fields have to obey the equations

$$(\nabla \times \mathbf{B}) \times \mathbf{B} = \mathbf{0}, \quad (1)$$

$$\nabla \cdot \mathbf{B} = 0. \quad (2)$$

We define the functional

$$L = \int_V \left[w_a \, B^{-2} \, |(\nabla \times \mathbf{B}) \times \mathbf{B}|^2 + w_b \, |\nabla \cdot \mathbf{B}|^2 \right] \, d^3x, \quad (3)$$

where w_a and w_b are weighting functions. It is obvious that (for $w_a, w_b > 0$) the force-free equations (1-2) are fulfilled when L is equal zero. We minimize the functional (3) with an iterative scheme:

$$\frac{\partial \mathbf{B}}{\partial t} = \mu \tilde{\mathbf{F}}, \quad (4)$$

which (for $\mu > 0$) ensures that L is monotonically decreasing. See Wiegelmann (2004) for the definition of $\tilde{\mathbf{F}}$ for the case of one weighting function ($w_a = w_b = w$). A generalization towards two weighting functions is

straight forward (see appendix A). The method has been developed by Wheatland et al. (2000) for the case without weighting function. Our code reduces to this approach for the choice $w_a = w_b \equiv 1$ in the entire box. The weighting functions are useful if only the bottom boundary data are known. In this case we introduce a buffer boundary of several grid points towards the lateral and top boundary of the computational box. The weighting functions are chosen constant in the inner, physical domain and drop to 0 with a cosinus-profile in the buffer boundary towards the lateral and top boundary of the computational box (see Wiegelmann (2004) for details). In most cases the weighting functions w_a and w_b are chosen identically $(w_a = w_b = w)$, which gives the same weighting to the force-free and solenoidal condition.

2.2. Implementation

The method works as follows:

1. Compute start equilibrium (e.g. a potential field) in the computational box.
2. Replace the bottom boundary (or all six boundaries) with the vector magnetogramm.
3. Minimize the functional (3) with the help of Eq. (4). The continuous form of (4) guaranties a monotonically decreasing L. This is as well ensured in the discretized form if the iteration step dt is sufficiently small. The code checks if $L(t + dt) < L(t)$ after each time step. If the condition is not fulfilled, the iteration step is repeated with dt reduced by a factor of 2. After each successful iteration step we increase dt slowly by a factor of 1.01 to allow the time step to become as large as possible with respect to the stability condition.
4. The iteration stops if L becomes stationary. Stationarity is assumed if $\frac{\partial L}{\partial t}/L < 1.0 \cdot 10^{-4}$ for 100 consecutive iteration steps.

The program is written in C and has been parallelized with OpenMP.

3. TESTS AND PERFORMANCE

The optimization method has been tested with help of the semi-analytic solution by Low & Lou (1990) for small boxes in Wheatland et al. (2000) and Wiegelmann and Neukirch (2003) showed that the optimization principle is faster and gives higher accuracy than MHD relaxation. Here, we demonstrate that the method can be as well be applied to larger boxes, where the largest box used contained 256^3 grid points. By theoretical investigations Wheatland et al. (2000) predicted that the method has 5th order and consequently doubling the resolution leads to an increase in computing time by a factor of 32. We checked the performance explicitly in Fig. 1 for different box size and found that the computing time increases with a potence of 5.4. Let us remark that the computer was also busy with other programs during the computation of the largest box (256^3 grid points, 14 days) which slowed down our computation.

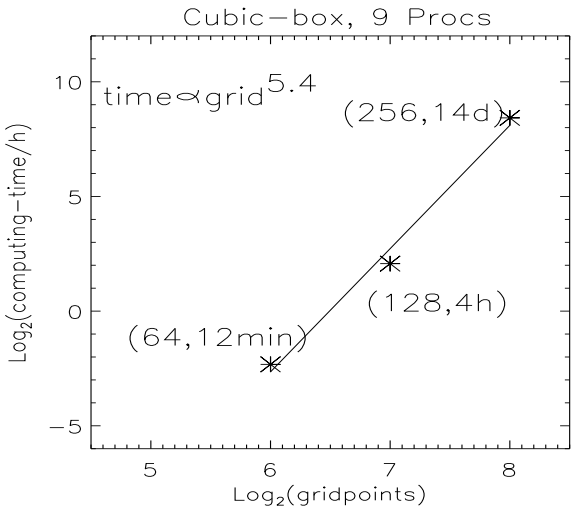

Figure 1. Performance of the optimization principle. We carried out computations with cubic boxes of 64^3, 128^3 and 256^3 grid points on a 9 processor parallel computer. Both axes are in logarithmic scaling.

The result of our computation is shown for the 128^3 box in Fig. 2. Panel a) shows the original Low and Lou solution and panel b) the reconstruction with our code. A reasonable agreement is obvious. For comparison we show a corresponding potential field (to the same line of sight photospheric magnetic field) in panel c).

3.1. Magnetic energy

For the prediction of a magnetic configuration is likely to erupt soon two quantities are assumed to play and important role, the magnetic energy and the magnetic helicity. It is therefore important to check, if the code get's these quantities correct. The magnetic energy is defined as

$$E_{\mathrm{mag}} = \frac{\int B^2 \, d^3x}{2\mu_0} \tag{5}$$

To get some information about the free energy of a configuration we compute the energy compared with the energy of a potential field, which corresponds to the minimum energy state for a given photospheric flux. The magnetic energy of the the original Low and Lou field is 1.51 the energy of the potential field. Our force-free code computes the energy to 1.49 the energy of the potential field which corresponds to an error of 1.3%. This seems to be acceptable.

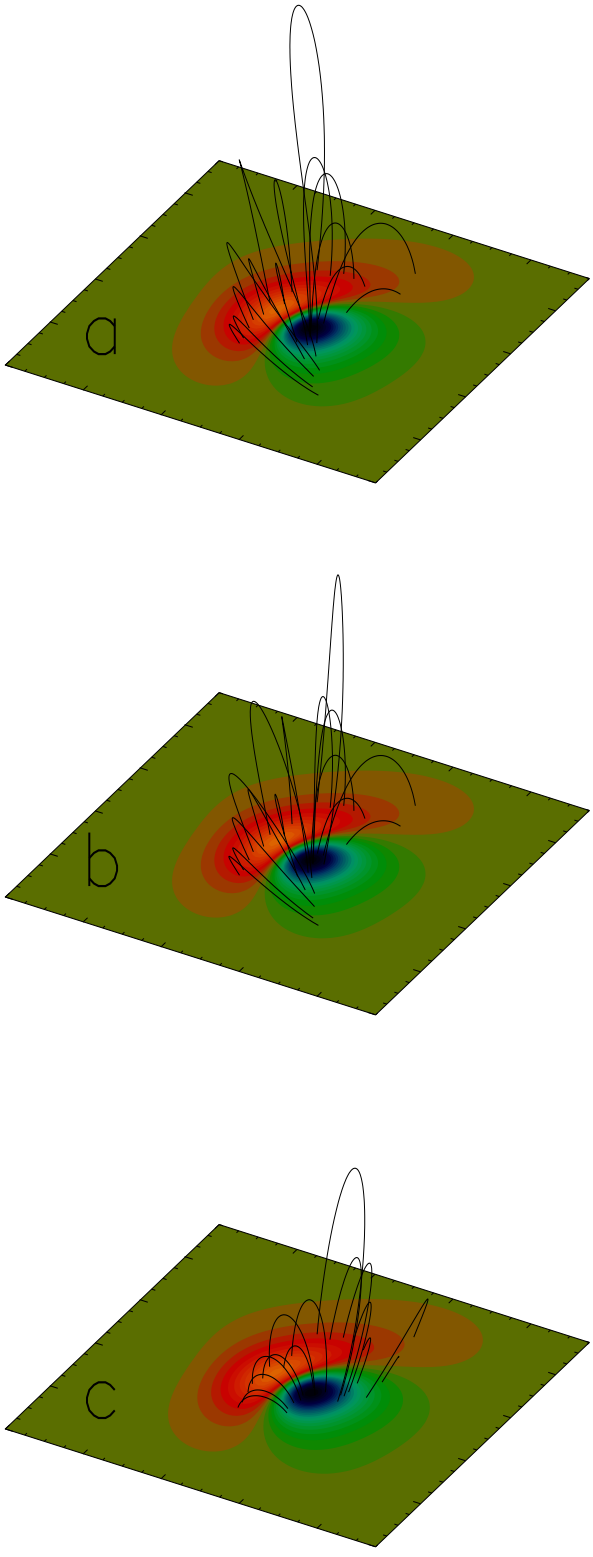

Figure 2. Panel (a) shows the original Low and Lou solution, panel (b) a non-linear force-free extrapolation and panel (c) a potential field. It is obvious that the non-linear force-free approach agrees with the original much better. The computation was done in a 128^3 *computational box including a boundary layer of* 16 *points towards the lateral and top boundaries of the computational box.*

3.2. Magnetic helicity

The magnetic helicity is defined as

$$H = \int \mathbf{A} \cdot \mathbf{B} d^3x \tag{6}$$

Unfortunately this definition is not gauge invariant. It is only gauge invariant for an isolated volume with no magnetic flux through the boundaries of the volume. Configurations with this feature are useful for theoretical investigations, but not fulfilled for coronal magnetic fields. Active regions are not isolated, but of course connected with the photosphere and the reconstructed force-free magnetic fields have certainly magnetic flux through the photospheric boundary and in most cases also through the lateral and top boundary of the computational box. It is therefore important to find a gauge invariant definition of the magnetic helicity for this general case. Such a definition was given in Schindler et al. (1988) and called relative magnetic helicity:

$$H_{\mathrm{mag}} = \int (\mathbf{A} + \mathbf{A_0}) \cdot (\mathbf{B} - \mathbf{B_0}) d^3x \tag{7}$$

where $\mathbf{A}$ is the magnetic vector potential and $\mathbf{A_0}$ and $\mathbf{B_0}$ correspond to the potential field. The relative magnetic helicity is gauge free. Relative means relative to a corresponding potential field and a potential field has per definition a relative magnetic helicity of 0.

The relative magnetic helicity is -0.94 for the original Low and Lou field and -1.00 for the force-free extrapolation which corresponds to and error of 6.0%. We normalize the magnetic helicity with

$$B^2 \; L_{\mathrm{ave}} \tag{8}$$

where L_{ave} is the average box length.

Our reconstruction code not uses the vector potential explicitly and we compute $\mathbf{A}$ from the reconstructed force-free magnetic field together with the Coulomb gauge condition

$$\nabla \cdot \mathbf{A}. \tag{9}$$

Let us remark that we use a preliminary version to compute the vector potential, which might be improved in future.

3.3. Evaluation of the test

The comparison with a known analytic non-linear force-free solution demonstrated that our code works correct. We find a good agreement of the original solution and the reconstructed field. We got a reasonable agreement of the topology of the magnetic field lines as well as for the magnetic energy and magnetic helicity. Consequently we conclude that we can extrapolate a non-linear force-free coronal magnetic field from photospheric vector magnetograph observations. We applied our code to

data from VTT and compared the reconstruction result with chromospheric measurements in Wiegelmann et al. (2005) and found a reasonable agreement for non-linear force-free fields.

4. APPLICATION

In the following we apply our method to vector magnetograph data from IVM and SFT.

4.1. AR7986 taken with IVM in Hawaii

We apply the reconstruction code to IVM-data for active region $AR7986$ taken on 28. August 1996. Fig. 3 a) shows a potential field reconstruction and Fig. 3 b) a non-linear force-free reconstruction. The non-linear force-free magnetic field line plots in Fig. 3 b) show a deviation from the potential field in Fig. 3 a) but the deviation is rather small. The magnetic energy of the force-free field is a factor of 1.16 higher compared with a corresponding potential field and has a positive helicity (0.25 normalized with $B^2\ L_{\rm ave}$). The small value of the magnetic energy (only 16%) higher than the magnetic energy of a potential field, the small helicity as well as the magnetic field line plots suggest, that the configuration is close to a potential field. To compare the magnetic field lines of the potential field with the non-linear force-free field we fixed the locations of the photospheric footpoints at positive flux. Despite the similarity of the majority of the field lines in Fig. 3 a) and b) there are some topological differences. In the potential field a small positive spot close at the right front is connected with a tiny loop to a nearby negative flux region, but for the non-linear force-free field in 3 b) the same spot is connected with the far away negative flux region in the left.

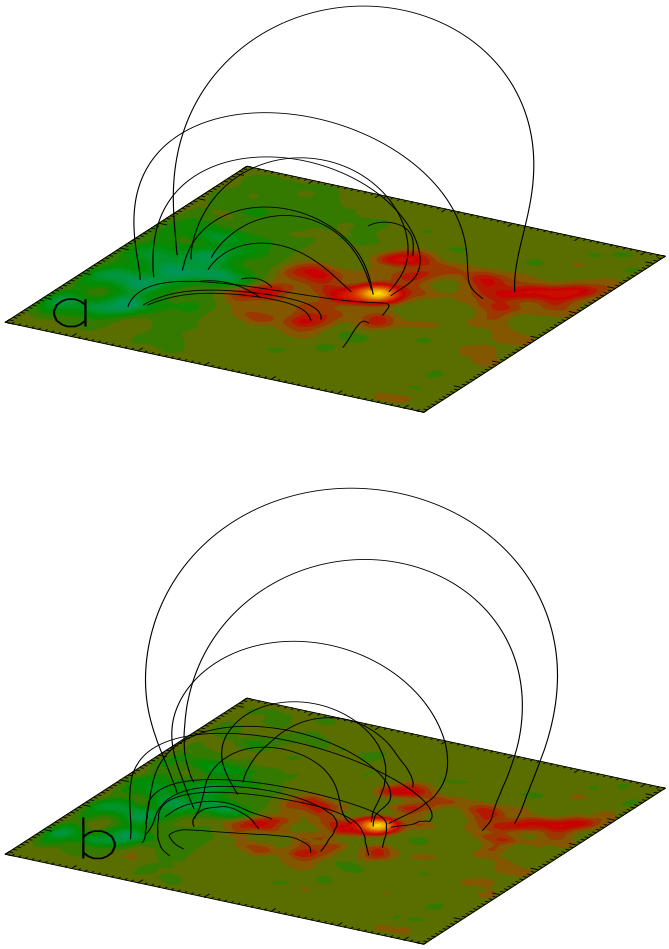

Figure 3. AR7986 taken on 28. August 1996 with IVM. Panel (a) shows a potential field reconstruction and panel (b) a non-linear force-free extrapolation. The computation was done in a $96 \times 96 \times 80$ computational box including a boundary layer of 16 points towards the lateral and top boundaries of the computational box (boundary layer not shown in the image).

4.2. AR7321 taken with SFT in Tokyo

Table 1. Time evolution of AR7321. See also Fig. 4.

Time	$\frac{E_{\rm mag}}{E_{\rm pot}}$	$\frac{H_{\rm mag}}{B^2\,L_{\rm ave}}$
26/10/92	1.41	-0.16
27/10/92	1.30	+1.90

Fig. 4 shows the time evolution of Active region AR7321. The photospheric vector magnetic field was taken with the Solar Flare Telescope (SFT) in Tokyo on 26th and 27th october 1992 and we applied our non-linear force-free extrapolation code to compute the 3D magnetic field structure. A visual inspection of the right panels of Fig. 4 reveal that the magnetic configuration changed significantly from the 26th to 27th october. From Tab. 1 we see that the total and relative magnetic energy as well as the magnetic helicity changed, too.

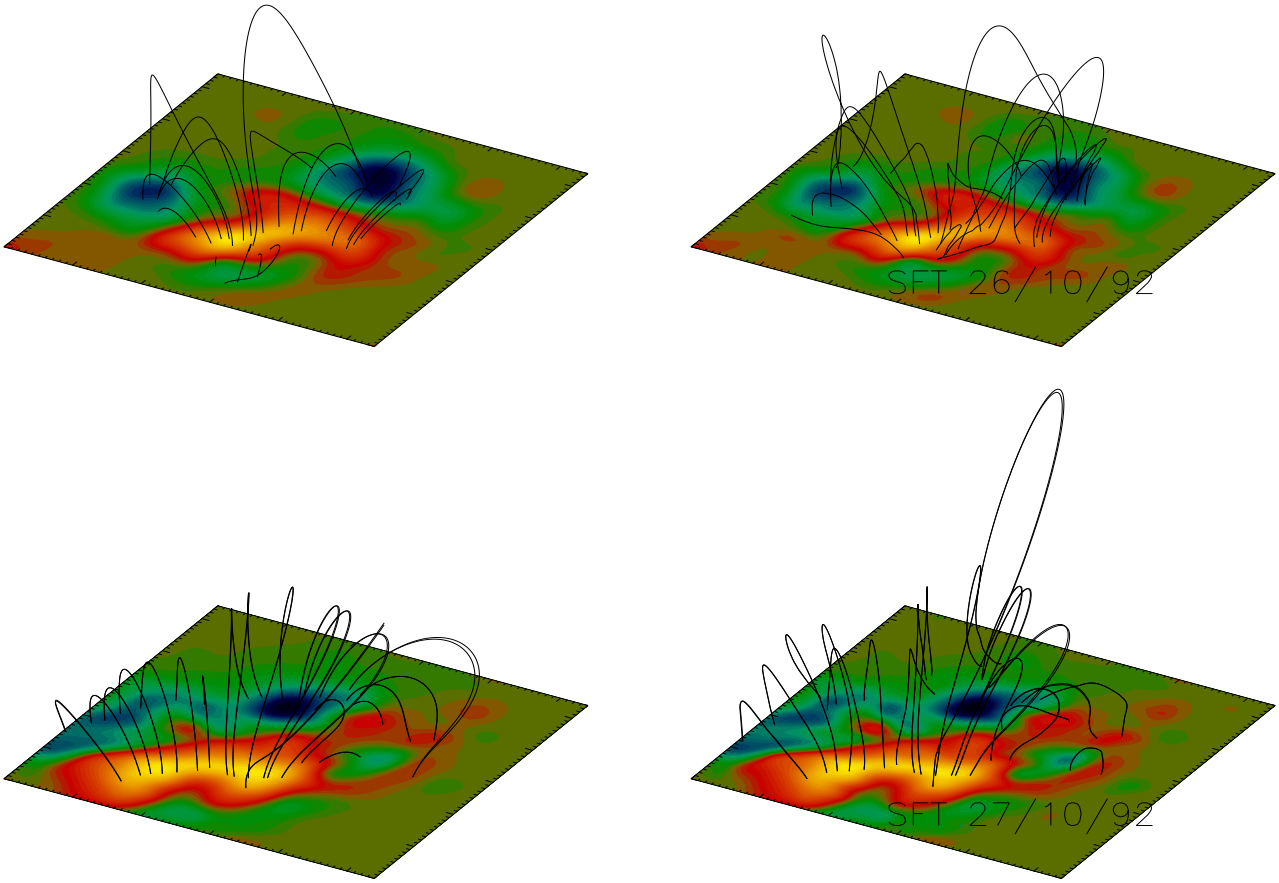

Figure 4. Time evolution of AR7321, non-linear force-free computations with vector magnetogram data from SFT in Tokyo. The computation was done in a $75 \times 75 \times 65$ *computational box including a boundary layer of* 10 *points towards the lateral and top boundaries of the computational box. The left-hand pictures are a potential field reconstruction and the right-hand pictures a non-linear force-free reconstruction.*

5. CONCLUSIONS

We described a computer program for the computation of non-linear force-free fields from photospheric vector magnetograms. We tested our code with the help of a semi- analytic equilibria and found a good agreement. The performance test also revealed that the present version of the code can handle moderately large computational boxes up to approximately 256^3 grid points on a parallel computer which required 3.2 GB of free memory. We applied our code to data from IVM in Hawaii and SFT in Tokyo. In future we are also planning to use data from SOLIS and Solar-B. A current problem of non-linear force-free modelling is that the required vector magnetograph data are often not available or have a limited field of view. This will hopefully change in the nearest future as soon as data from the full disc vector magnetograph SOLIS become available. The current version of the code is written in Cartesian coordinates and applications are mainly dedicated to active regions. In principle it would be desired to write the code as well in spherical coordinates to get a global non-linear force-free coronal magnetic field model. One has to think in advance however, how to deal with the fast increasing computing time (5th order) which makes it hard to handel very large computational boxes.

A. MATHEMATICAL APPENDIX

With

$$\mathbf{\Omega_a} = B^{-2}\,(\nabla\times\mathbf{B})\times\mathbf{B} \quad (A.10)$$

$$\mathbf{\Omega_b} = B^{-2}\,(\nabla\cdot\mathbf{B})\,\mathbf{B}. \quad (A.11)$$

the functional reads:

$$L=\int_V w_a\,B^2\Omega_a^2+w_b\,B^2\Omega_b^2\,d^3x, \quad (A.12)$$

We minimize equation (A.12) with respect to an iteration parameter t and obtain an iteration equation for the magnetic field

$$\Rightarrow\frac{1}{2}\,\frac{dL}{dt}=-\int_V\frac{\partial\mathbf{B}}{\partial t}\cdot\tilde{\mathbf{F}}\,d^3x-\int_S\frac{\partial\mathbf{B}}{\partial t}\cdot\tilde{\mathbf{G}}\,d^2x \quad (A.13)$$

$$\tilde{\mathbf{F}} = \tilde{\mathbf{F_a}}+\tilde{\mathbf{F_b}} \quad (A.14)$$

$$\tilde{\mathbf{G}} = \tilde{\mathbf{G_a}}+\tilde{\mathbf{G_b}} \quad (A.15)$$

$$\tilde{\mathbf{F_a}} = w_a\,\mathbf{F_a}+(\mathbf{\Omega_a}\times\mathbf{B})\times\nabla w_a \quad (A.16)$$

$$\tilde{\mathbf{F_b}} = w_b\,\mathbf{F_b}+(\mathbf{\Omega_b}\cdot\mathbf{B})\,\nabla w_b \quad (A.17)$$

$$\tilde{\mathbf{G_a}} = w_a\,\mathbf{G_a} \quad (A.18)$$

$$\tilde{\mathbf{G_b}} = w_b\,\mathbf{G_b} \quad (A.19)$$

$$\mathbf{F_a} = \nabla\times(\mathbf{\Omega_a}\times\mathbf{B}) - \mathbf{\Omega_a}\times(\nabla\times\mathbf{B})+\Omega_a^2\,\mathbf{B} \quad (A.20)$$

$$\mathbf{F_b} = \nabla(\mathbf{\Omega_b}\cdot\mathbf{B})-\mathbf{\Omega_b}(\nabla\cdot\mathbf{B})+\Omega_b^2\,\mathbf{B} \quad (A.21)$$

(A.22)

$$\mathbf{G_a} = \hat{\mathbf{n}}\times(\mathbf{\Omega_a}\times\mathbf{B}) \quad (A.23)$$

$$\mathbf{G_b} = -\hat{\mathbf{n}}(\mathbf{\Omega_b}\cdot\mathbf{B}) \quad (A.24)$$

and $\hat{n}$ is the inward unit vector on the surface S. The surface integral in (A.13) vanishes if the magnetic field is described on the boundaries of a computational box (boundary layer not shown in the image).

ACKNOWLEDGMENTS

We acknowledge use of data from IVM in Hawaii and SFT in Tokyo. This work was supported by DLR-grant 50 OC 0007.

REFERENCES

Amari, T., Boulmezaoud, T. Z., Mikic, Z.: 1999, A&A, 350, 1051.

Chiu, Y.T., Hilton, H.H.: 1977, ApJ, 212, 821.

Low, B. C., & Lou, Y. Q. 1990, *ApJ*, 352, 343

Sakurai, T.: 1981, Sol. Phys., 69, 343.

Schindler, K., Hesse, M., & Birn, J. 1988, *JGR*, 93, 5547

Schmidt, H.V.: 1964 in W.N. Ness (ed.), *ASS-NASA Symposium on the Physics of Solar Flares*, NASA SP-50, p. 107.

Seehafer, N.: 1978, Sol. Phys., 58, 215.

Semel, M.: 1967, Ann. Astrophys. ,30, 513.

Valori, G., Kliem, B., & Keppens, R. 2005, A&A, 433, 335

Wheatland, M. S., Sturrock, P. A., Roumeliotis, G.: 2000, ApJ., 540, 1150.

Wheatland, M. S. 2004, Sol. Phys., 222, 247

Wiegelmann, T. and Neukirch, T.: 2003, *Nonlinear Processes in Geophysics*, **10**, 313-322

Wiegelmann, T. 2004, Sol. Phys., 219, 87.

Wiegelmann, T., Lagg, A., Solanki, S. K., Inhester, B., & Woch, J. 2005, A&A, 433, 701

Yan, Y. and Sakurai, T.: 2000, *Solar Phys.* **195**, 89.